



**Synthesis of  $\text{TiC}(1-x)\text{--ZrC}_x$  ( $x=0.2$ ) composite by FAST-SPS-FCT technology, effect of SWCNTs and nano-WC additions on structural properties:  
Application for ballistic protection**

Badis Bendjemil, Safi Khaoula, Ilyas Kouahla, Mohamed Mouyane, Mustapha Arian, Jérôme Bernard, Frédéric Bernard, Dominique Vrel, Jacques Noudem, David Houivet

► **To cite this version:**

Badis Bendjemil, Safi Khaoula, Ilyas Kouahla, Mohamed Mouyane, Mustapha Arian, et al.. Synthesis of  $\text{TiC}(1-x)\text{--ZrC}_x$  ( $x=0.2$ ) composite by FAST-SPS-FCT technology, effect of SWCNTs and nano-WC additions on structural properties: Application for ballistic protection. Experimental and Theoretical Nanotechnology, 2023, pp.461-480. 10.56053/7.3.463 . hal-04299388

**HAL Id: hal-04299388**

**<https://hal.science/hal-04299388v1>**

Submitted on 22 Nov 2023

**HAL** is a multi-disciplinary open access archive for the deposit and dissemination of scientific research documents, whether they are published or not. The documents may come from teaching and research institutions in France or abroad, or from public or private research centers.

L'archive ouverte pluridisciplinaire **HAL**, est destinée au dépôt et à la diffusion de documents scientifiques de niveau recherche, publiés ou non, émanant des établissements d'enseignement et de recherche français ou étrangers, des laboratoires publics ou privés.



Distributed under a Creative Commons Attribution 4.0 International License



# Synthesis of $\text{TiC}_{(1-x)}\text{-ZrC}_x$ ( $x=0.2$ ) composite by FAST-SPS-FCT technology, effect of SWCNTs and nano-WC additions on structural properties: Application for ballistic protection

Badis Bendjemil<sup>1,3,5,6,\*</sup>, Khaoula Saft<sup>2</sup>, Ilyas Kouahla<sup>2</sup>, Mathias Moser<sup>4</sup>, Mohamed Mouyane<sup>5</sup>, Mustapha Arian<sup>4</sup>, Jérôme Bernard<sup>5</sup>, Frédéric Bernard<sup>4</sup>, Dominique Vrel<sup>3</sup>, Jacques Guillome Noudem<sup>6</sup>, David Houivet<sup>5</sup>

<sup>1</sup>Laboratory of applied mechanic and novel nanomaterials, University of 08 May 1945 Guelma, avenue 19 May 1956, CS 401, 24000 Guelma, Algeria

<sup>2</sup>LMS Laboratory, University of 8 May 1945 Guelma, avenue 19 May 1956, CS 401, CS 24000 Guelma, Algeria

<sup>3</sup>Laboratoire des Sciences des Procédés et des Matériaux – UPR 3407, 99 av. Jean-Baptiste Clément, CS 93430 Villetaneuse, Paris, France

<sup>4</sup>Laboratoire ICB, Procédés Métallurgiques et Durabilité des Matériaux, Institut Marey – Maison de la Métallurgie, 64 Rue de Sully, CS 21000 Dijon, France

<sup>5</sup>LUSAC, EA 4253, 60 rue Max Pol Fouchet, CS 20082, Université de Caen Basse-Normandie (UCBN), CS 50130 Cherbourg-Octeville, France

<sup>6</sup>ENSICAEN, 6, Boulevard Maréchal Juin, CS 45053, 14050 Caen Cedex 04, France

\*) Email: [Badis23@ymail.com](mailto:Badis23@ymail.com)

Received 27/3/2023, Accepted, 21/6/2023, Published 15/7/2023

This paper describes the SWCNTs and nano WC when were introduced into  $\text{TiC}_{(1-x)}\text{-ZrC}_x$  with ( $x=2$ ) nano-composite into ceramics to improve the fracture toughness ( $K_{IC}$ ) and hardness (Hv).  $\text{TiC-ZrC}$ ,  $\text{TiC-ZrC}$ -single walled carbon nanotubes (SWCNTs) (3 mass %) and  $\text{TiC-ZrC-SWCNTs}$  (3 mass %) - tungsten nanocarbide (NWC) (20 mass %) nano-composites were prepared by vacuum sintering FAST-SPS-FCT technology at the temperatures in the range of 1700–1800 °C for 400 s under pressure of 50 Mpa. Microstructural properties were investigated by X-ray diffraction and energy-dispersive spectrometry in addition scanning electron microscopy. The investigations shows that the phase

separation of the as-sintered (Ti, Zr) C into two phases: TiC-rich (Ti, Zr) C (dark) and ZrC-rich (Zr, Ti) C (bright) indicating that the as-sintered (Ti, Zr) C was thoroughly decomposed into two solid phases after sintering. The effect of nanostructures of SWCNTs and NWC is already illustrated. X-ray diffraction and energy-dispersive spectrometry results indicate that bright grains are (Zr, Ti) C solid solution. The relative density increases with the addition of SWCNTs and nano-WC content.

Fully dense TiC-ZrC, TiC-ZrC-SWCNTs and TiC-ZrC-CNTs-NWC nanocomposites with a relative density of more than 98 % were obtained. The Vickers hardness (HV) and fracture toughness ( $K_{IC}$ ), of TiC-based nano-composites with SWCNTs and NWC will be performed in the near future. In addition, ballistic performance (the properties of shock resistance); thermo-mechanical modelling in-situ FAST-SPS-FCT cycle, also will be evaluated using the Rosenberg model and compared with the experimental results in order to better understand the shock behavior of nano-composites that to be applied for body armor.

---

**Keywords:** FAST-SPS-FCT technology; TiC-based nano-composite; Microstructure and Mechanical properties.

## 1. INTRODUCTION

In a current context of decreasing polluting emissions, decreasing operating costs and increasing vehicle autonomy, the reduction of structures has become a major challenge for the industry. In the field of defence, ballistic protection necessary to guarantee the physical integrity of the occupants involve a substantial addition of mass which is detrimental to the mobility and autonomy of the vehicles. Efforts are therefore focused on the development of more efficient and lighter protection systems that are accompanied by general of an additional cost. The systems selected are called "double hardness", composed of surface masses of several shielding systems sufficient to stop a piercing ammunition compared to their relative cost [1] of a hard layer on the front face intended to deform the projectile and a more ductile layer to stop the fragments. Aluminum alloys, some of which are currently used in ballistic protection, stand out as one of the lightest metallic materials and have a good deformation capacity to absorb the kinetic energy of fragments (projectile and armor) by deformation. The choice of  $B_4C$  boron carbide ceramic because of its very high hardness (3rd hardest material after diamond and BN boron nitride [2]) and its low density ( $2.52 \text{ g/cm}^3$ ). To increase the mechanical properties of aluminium, several ways are considered: the composition of the alloy, its metallurgical state, the process used and the size of the resulting grains.

Finally, it is also possible to include hard ceramic type particles. The Al-Zn-Mg type composition because this alloy belongs to a family of structural hardening alloys [3]. As far as the process is concerned, the powder route was chosen because it makes it possible to obtain ultrafine grains and to integrate reinforcements without any problem of wettability [4].

Since  $B_4C$  is light and used in the field of ballistic protection [5], it is particles of this nature that will be introduced to produce composites with a metal matrix. Optimization of the grinding time of an Al-Zn-Mg powder to obtain a nanostructured material. Then, the study of the microstructure modifications induced during the consolidation by FAST-SPS-FCT technology. The mechanical properties were also evaluated under quasi-static and dynamic conditions.

The analytical models will make it possible to quantify the contributions to the reinforcement and the study of the interest of grinding during the development of the metallic material by way of powders. The ballistic impact resistance properties will be evaluated a priori using the Rosenberg model.

TiC or Ti(C, N) based cermets have drawn great attention as high-speed cutting tools to replace the traditional WC–Co alloys due to their high hardness, good wear resistance, good oxidation resistance, low thermal expansion coefficients and low expense [6, 7]. However, the lower toughness, thermal shock resistance and mechanical shock resistance of the TiC or Ti(C, N) based cermets limit their application in heavy turning and interrupt milling [8, 9]. Previous study shows that ZrC addition into TiC–TiN–WC–Ni–Co cermets can improve fracture toughness clearly due to the increased amount of the coreless grains, the spinodal decomposition in cermets, as well as the crack deflection and crack branching mechanisms [9].

Although spark plasma sintering (FAST-SPS-FCT technology) is often employed to consolidate refractory carbides, monolithic fully dense ZrC and TiC; there are difficult to obtain by another method. The FAST-SPS-FCT technology provides their skill in the field [10, 11, 12].

Other researchers described the multicomponent high entropi [38] ceramic solid solutions based on carbides of group IV–VI transition metals are of considerable scientific and practical interest due to their excellent physical and mechanical properties. An open question in this area is the formation of single-phase solid solutions from a mixture of metal carbides. They studied the phase evolution of equimolar powder mixtures of HfC–ZrC–TiC, HfC–ZrC–NbC, and HfC–ZrC–TiC–NbC during pressure sintering and showed that single-phase substitution solid solutions (Hf, Zr, Ti)C, (Hf, Zr, Nb)C, and (Hf, Zr, Ti, Nb)C based on hafnium carbide are formed in several [13].

Recent studies have shown that shear thickening behaviour of a concentrated dispersion of fumed silica particles in polyethylene glycol (PEG) under steady shear can be successfully utilized for ballistic protection [14 –19]. It has been demonstrated that composites made of Kevlar fabric reinforced by shear thickening fluid (STF) can offer equivalent low velocity ballistic performance similar to neat Kevlar, but with significantly fewer number of layers. Consequently, the resulting armor system is lighter and more flexible [20, 21].

In recent years, nanocomposites have emerged as new hybrid materials consisting of polymers and nanometer-sized inorganic particles. These nanocomposites have exhibited significant improvement in chemical, thermal, and mechanical properties with a very low loading of the inorganic particles, while still allowing conventional polymer processing. The benefit of nanoparticle infusion comes from the fact that the large amount of interphase zones in nanocomposites may serve as catalysts for prolific crack growth, creating a much greater number of new surfaces [22–24].

TiC based nanocomposite and binders' metals generally and usually used for cutting tools because of their mechanical properties (hardness and fracture toughness).

But in this paper TiC based composites were combined with the nanostructure of carbon nanotubes (SWCNTs) and tungsten nanocarbide (NWC) which improves his mechanical properties in order to study its ballistic behavior. It is tried for the first time in ballistic protection.

In this paper is presented first preliminary results from structural properties, phase and microstructural analysis and densification behavior of the composite TiC-ZrC with and without nanostructure of carbon nanotubes and tungsten nanocarbide. The ballistic performance will be investigated using the Rosenberg model and compared with the experimental results in order to better understand the shock behavior of nanocomposites that can be applied for ballistic performance.

## 2 EXPERIMENTAL

### 2.1 Starting Material

TiC (particle size: 1–2  $\mu\text{m}$ , Wako Pure Chemical, Osaka, Japan), ZrC (purity: 95%; Kojundo Chemical Laboratory, Sakado, Japan) powders were used as starting materials. The TiC and ZrC powders were mixed (ZrC composition of 20 vol%) and then ball-milled for 20 ks in an agate bottle using zirconia balls with a small amount of ethanol. The mixed powders were oven-dried at 340 K for 80 ks and passed through a 200-mesh sieve forming composite A. SWCNTs produced by HiPCO process and by laser ablation methods [25, 26, 27, 37] (nanostructure size: 1 nm, IFW-Spectroscopy Group-Dresden and TU-Dresden, Germany). Tungsten nano-carbide (NWC) (particle size: 4–8 nm, Goodfellow Pure Chemical, Germany). First 3 masses % of SWCNTs were introduced into 80 vol% TiC-20 vol% ZrC-3 mass% SWCNTs according to the steps described in [28, 29, 30, 31] forming nano-composite A; and then 20 masses % of NWC were also added to nano-composite A forming nano-composite B after ball-milling. The specimens were mirror-polished using diamond slurry (1  $\mu\text{m}$ ). The crystal phases and lattice parameters were examined by X-ray diffraction (XRD,  $\theta$ – $2\theta$ , Cu-K $\alpha$ , Bruker, Tokyo, Japan). Microstructures were observed by scanning electron microscopy (SEM, Hitachi, Tokyo, Japan). The HV and  $K_{IC}$  values were measured at room temperature by a Vickers hardness tester (HM-221, Mitutoyo, Tokyo, Japan) at load 1.96 N.  $K_{IC}$  will be calculated from Eq. (1) [32]:

$$K_{IC} = 0.016(E/H_v)^{1/2}(P/c^{3/2}) \quad (1)$$

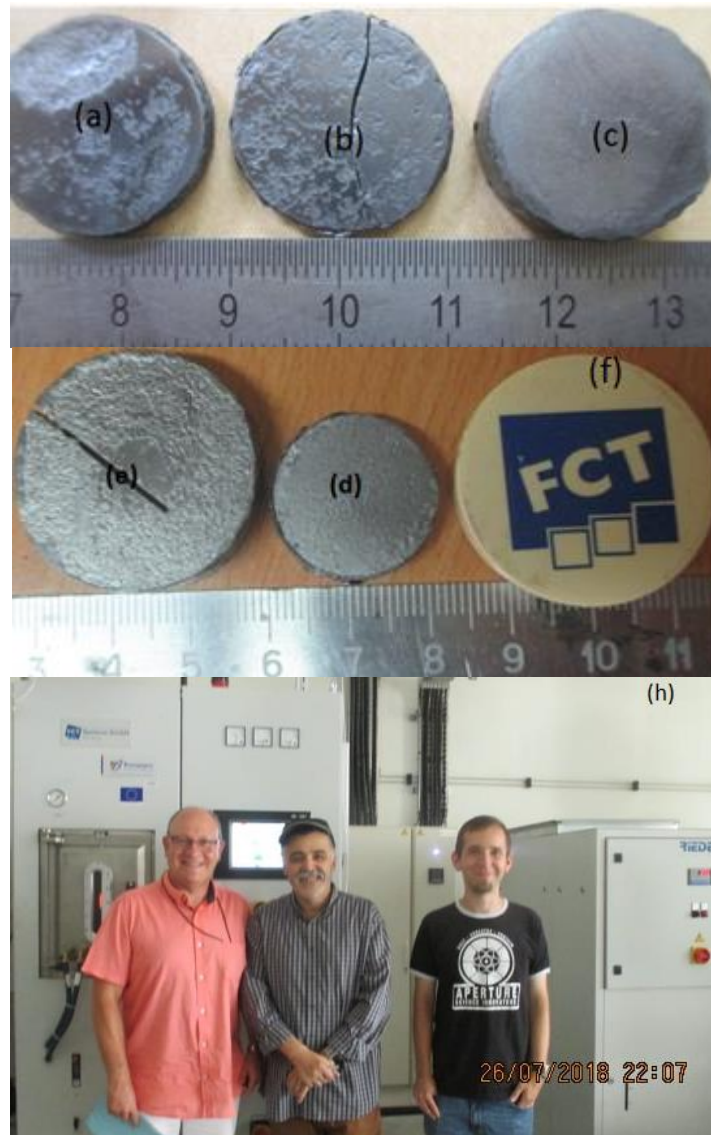
where E is Young's modulus and c is the half lengths of the crack formed around the corners of indentation. Young's moduli of TiC and ZrC are 470 and 400 GPa, respectively, and Young's moduli of the composites were estimated by the rule of mixtures.

### 2.2. Synthesis of composite and nanocomposites by FAST-SPS-FCT technology

**Consolidation of Powders via Spark Plasma Sintering** The field assisted sintering Technique-Spark Plasma Sintering technology (FAST-SPS-FCT) technology is an effective technique for the compaction of powder materials. A main characteristic of this method is the direct heating of the pressing tool and/or the sample by pulsed direct electrical current with low voltage. This results in high heating rates and allows for short treatment times in order to obtain highly compacted sinter bodies. The material transport (e.g. by diffusion) occurring during the sintering process can also be used for performing chemical reactions. Especially the conditions during the FAST-SPS process allow the use of the method also as an alternative synthesis route for nano-composites, of which, some can be obtained only with difficulties by other techniques. The ball-milled powders were consolidated via FAST-SPS-FCT method under high vacuum conditions using graphite die and punch at an applied external pressure of 50 MPa. In order to prepare high density compacts with negligible porosity, temperature and compression pressure was programmed to rise simultaneously,

until stabilized to the maximum temperature and compression pressure, followed by holding the system at the same sintering conditions for 1.6 ks. Circular compacts with diameter 20 mm and thickness 4 mm were prepared using FAST- SPS-FCT. The sintering conditions used in this study are provided in Table 1. The five sintering schedules are represented in the (Fig.2).

The resulting samples of the TiC- based nano-composites were sintered by FAST-SPS-FCT in graphite dies (inner diameter of 20 mm) coated with graphite sheet lubricant atomized with cBN at 1273 to 1473°K in vacuum. The Table 1 presented the sintering condition of the TiC-based nano-composites. The applied pressure 50 MPa was adjusted to the powder at room temperature and kept constant throughout the hot-pressing process. The pressure was applied at the beginning of the sintering process because high green density is favorable for better densification rate by reducing the pores prior to the densification during heating. The heating rate was about 10°C/min and the dwelling time at terminal temperature was 60 min. The temperature was measured by an infrared pyrometer through a hole opened in the graphite die. Furthermore, for monitoring densification process, the shrinkage of the powder compact was measured by a displacement sensor during the sintering. The dimensions of the finally sintered samples were about 20 mm in diameter and 3 mm in thickness after calculation of their weight using the densities values. The mixtures were loosely compacted into a graphite die of 20 mm in diameter and sintered in the vacuum (1 Pa) at various temperatures using an FAST-SPS-FCT apparatus at the sinter Labs: Laboratoire Interdisciplinaire Carnot de Bourgogne (ICB), 9 AV Alain Savary, 21000 Dijon- France (Fig.1).

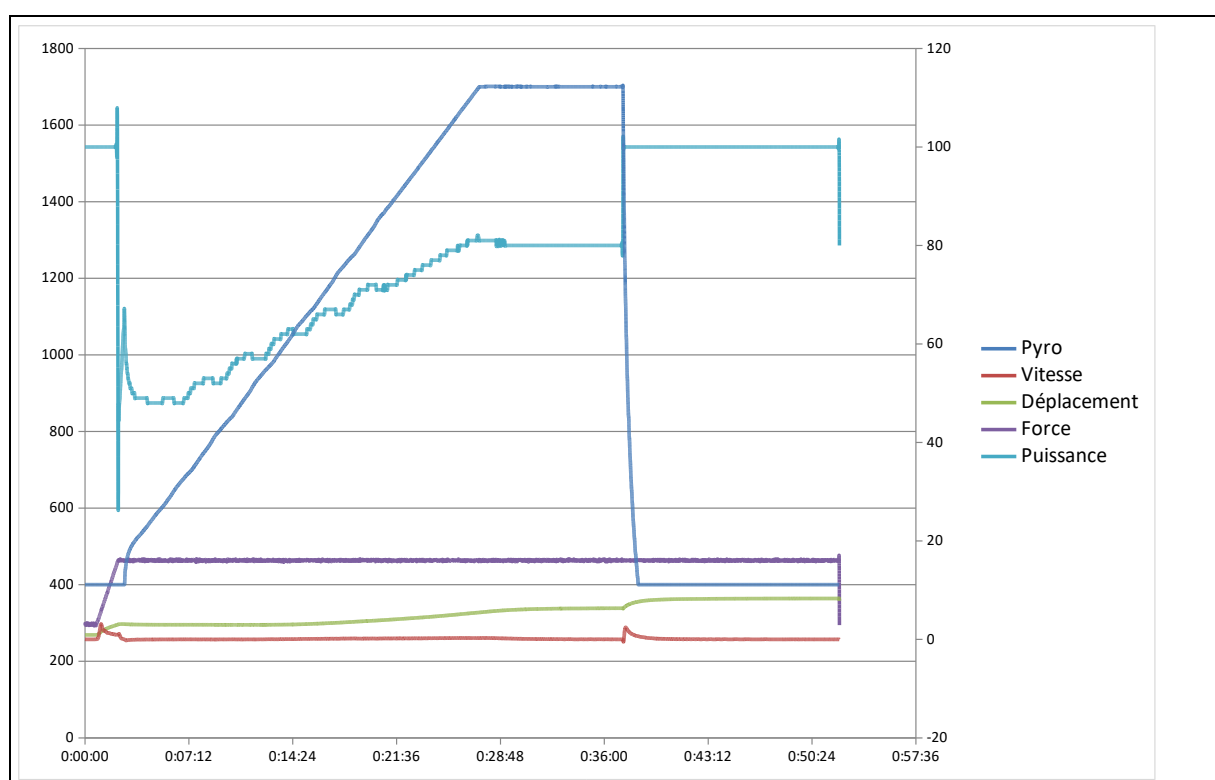


**Figure 1** Sintered samples with die diameter of 20 mm: **(a)** Nano-composite A, **(b)** Nano-composite B, **(d)** Composite A, **(c)** TiC with die of 20 mm, **(e)** TiC with die of 30 mm, **(f)** Swan of FAST-SPS-FCT apparatus-Germany, **(h)** FAST-SPS-FCT apparatus at the sinter Labs: Laboratoire Interdisciplinaire Carnot de Bourgogne, 9, AV Alain Savary, 21000 Dijon-France (Frédéric Bernard, Badis Bendjemil, Mathias Moser)

A constant heating rate of 120°C/min was employed, while the applied pressure was 50 MPa. The on/off time ratio of the pulsed current was set to 10/2 in each run. The maximum current reached approximately 3000 A during sintering. recorded in order to analyze the synthesis and sintering. The sintered samples are presented in the Figure 3. Densities of the sintered samples was measured by the Archimedes' using the densimeter type Micromeritics Accupyc 1330.

**Table 1** FAST-SPS-FCT technology synthesis parameters.

Sintred Samples	T (°C)	Time of the cycle (mn)	Heating rate (C/min)	P (MPa)	Mass % SWCNTs diameter=1 nm	Mass % NWC Size= 4–8 nm	Current (A)
TiC	1700	8	10	50	00		3440
ZrC	1700	8	10	50	00		3440
Composite A	1700	8	10	50	00		3440
Nano-composite B	1700	8	10	50	03		3440
Nano-composite C	1700	8	10	50		20	3440

**Figure 2** Variation of die displacement or shrinkage, temperature and applied pressure in dependence on the heating time during the FAST-SPS-FCT technology sintered samples.



The composite and nano-composites (denoted as A–A-B) were designed with different additions. The chemical compositions and the powder sizes of the nano-composites are listed in Table 2.

**Table 2** Chemical compositions and powder sizes of the designed composite and nano-composites.

Carbide Composite Nano-composite	TiC (1.99 $\mu\text{m}$ )	ZrC (0.88 $\mu\text{m}$ )	TiC-ZrC	TiC-ZrC-SWCNTs (1.00 nm)	TiC-ZrC-SWCNTs-NWC (4-6 nm)
Composite A			80(vol%)-20(vol%)		
Nano-composite A				80(vol%)-20(vol%)-3mass%	
Nano-composite B					80(vol%)-20(vol%)-3mass%-20mass%

The microstructure of polished specimen was observed by optical microscopy and scanning electron microscopy (SEM) in back scattered electron mode, in conjunction with an energy-dispersive spectrometry (EDS). The element distribution in different phases was characterized by EDS. The phase identification of the nano-composites was carried out by an X-ray diffractometer. The measurement of relative density was conducted by Archimedes method, which was described in previous literature [33].

### 3. RESULTS AND DISCUSSION

#### 3.1 Structural properties

##### 3.1.1 Densification behaviour

Densification of TiC–ZrC composites was examined by the displacement of a graphite punch during sintering, i.e., from shrinkage curves. Fig. 2 displays the effects of the nominal composition on shrinkage curves. at 400–1700 °C and the time dependence of isothermal displacements at 1700 °C up to 500 s. The displacement of the monolithic TiC occurred at lower temperature and was more significant than that of the monolithic ZrC, as shown in Fig. 2; the shrinkage of the monolithic TiC started at 1100 °C and proceeded up to 1700 °C, whereas the monolithic ZrC started to shrink above 1400 °C. For TiC–ZrC composites, the displacement in 80TiC–20ZrC composite A began at approximately 1100 °C and the composite gradually shrunk as the sintering temperature increased from 1100 to 1700 °C, as shown in Fig. 2.

##### 3.1.2 Phase formation of solid solutions of TiC–ZrC

The phase formation of solid solutions of TiC–ZrC Fig. 3 depicts the effects of additions on the XRD patterns of the 80TiC–20ZrC composite A. In the Fig. 3a reflection peaks of the

starting mixture powders, ZrC (JCPDS 35-0784) and TiC (JCPDS 65-0242), are included for comparison. At 1700 °C, the peak positions of TiC in the TiC–ZrC composite A (Fig. 3b) were slightly lower than those of the starting TiC powder. In contrast, the peak positions of ZrC were higher than those of the starting ZrC powder, as additions of (SWCNTs and nano. WC) are added, the peaks positions has no change (no shifting to the lower side from the positions of the starting TiC and to the higher side from the positions of the starting ZrC). The peak shifts of TiC reflections indicated the formation of Ti-rich (Ti, Zr) C accompanied by lattice expansions due to substitution of Zr into the Ti lattices and vice versa for the formation of Zr-rich (Ti, Zr) C. Relative intensities of Zr-rich peaks decreased with the additions. The relationship between the nominal compositions and lattice parameters of the single-phase (Ti, Zr) C. The lattice parameter linearly increased from 0.437 to 0.467 nm, which was consistent with Vegard's law (Table 4). This system is a complete solid solution and has an immiscibility dome below 2400 K (Fig.4). The 80TiC-20ZrC composite A solid solution sintered at 1700 °C had a uniform microstructure. This behaviour was in good agreement with the phase diagram in Fig. 4. The XRD patterns of the as-sintered (Ti, Zr) C composite and with additions like nano-composite A and B are the magnified peaks around 38-42 degree and 54-61 degree in Fig. 3b, respectively.

The XRD pattern of the as-sintered (Ti, Zr) C (Fig. 3b) exhibited a single set of reflection peaks assigned to a (Ti, Zr) C solid solution. Reflection peaks were identified at higher and lower angles compared with the original reflection peaks (Fig. 3b). This indicated the phase separation of the as-sintered (Ti, Zr) C into two phases: TiC-rich (Ti, Zr) C and ZrC-rich (Zr, Ti) C. indicating that the as-sintered (Ti, Zr) C was thoroughly decomposed into two solid phases. The NWC is dispersed in the matrix uniformly and had pics position with lower intensity (Fig.3b). Table 3 summarize the lattice parameters of the as-sintered (Ti, Zr) C and the two solid solutions (TiC-rich (Ti, Zr) C and ZrC-rich (Zr, Ti) C. On the basis of the lattice parameter of the as-sintered (Ti, Zr) C (0.437 nm), the composition was estimated as  $\text{Ti}_{0.91}\text{Zr}_{0.09}\text{C}$  by Vegard's law; this composition coincided with the nominal composition of the TiC and ZrC starting powders. The lattice parameters of TiC-rich (Ti, Zr) C and ZrC-rich (Zr, Ti) C were 0.435 and 0.468 nm, corresponding to  $\text{Ti}_{0.97}\text{Zr}_{0.03}\text{C}$  and  $\text{Zr}_{0.94}\text{Ti}_{0.06}\text{C}$ , respectively. These compositions were almost consistent with those of the binodal line in Fig. 4. The as-sintered (Ti, Zr) C exhibited the uniform morphology (Fig. 5c).

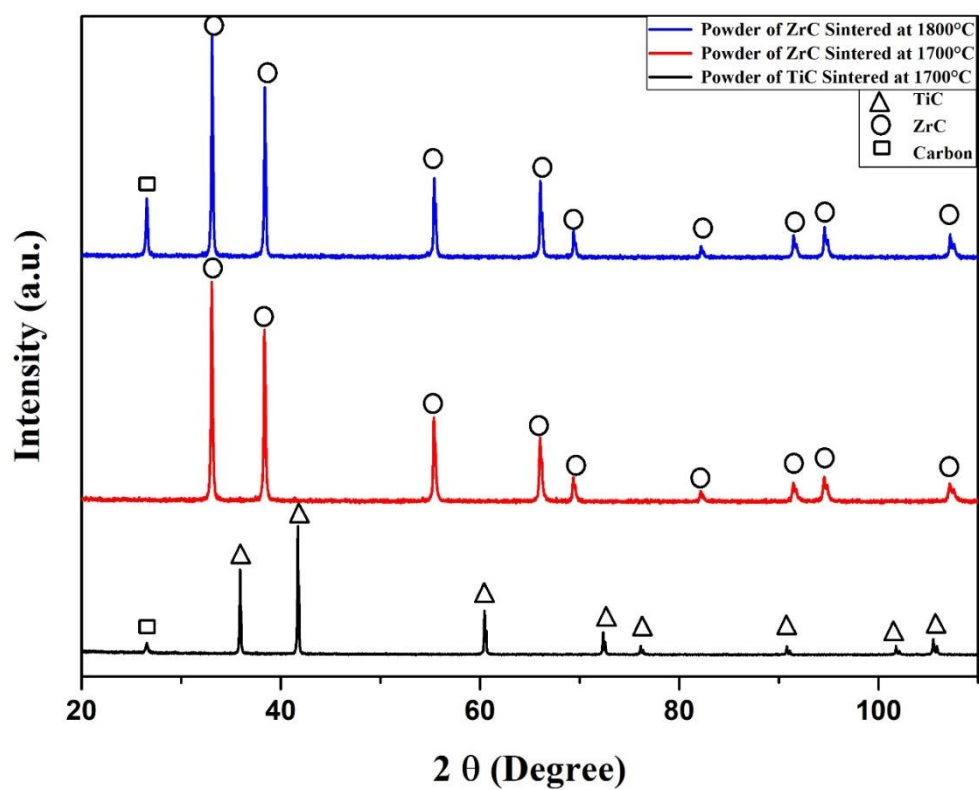


**Figure 3a** Spectra of TiC and ZrC carbides sintered by FAST-SPS-FCT technology at 1700 °C with die of 20 mm. are included for comparison.

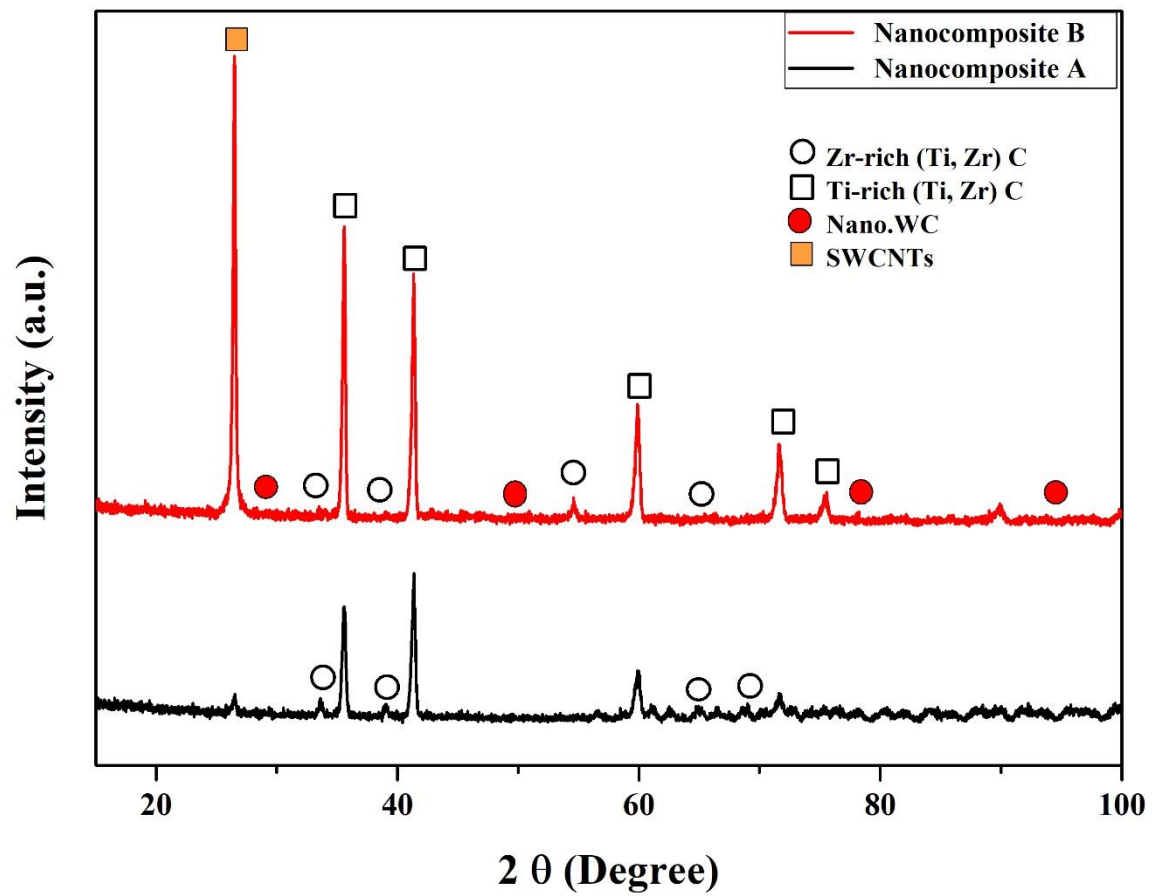


**Figure 3b** Effect of additions (SWCNTs, NWC) on the XRD patterns of the 80TiC–20ZrC composites A sintered by FAST-SPS-FCT technology at 1700 °C with die of 20 mm.

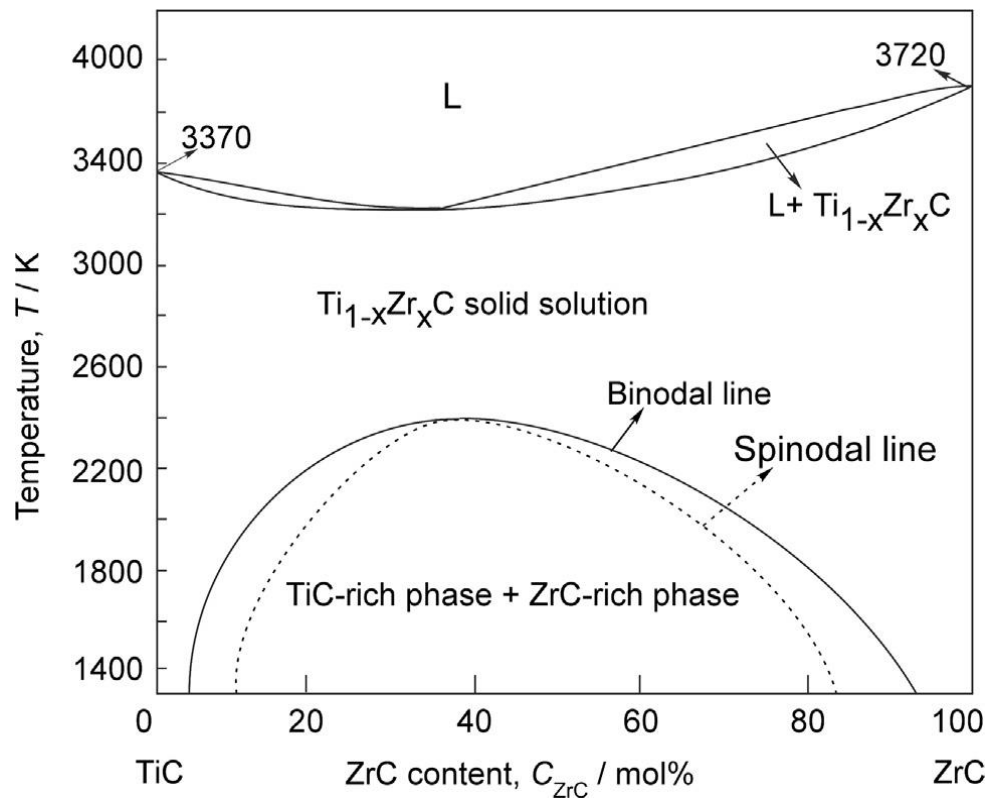
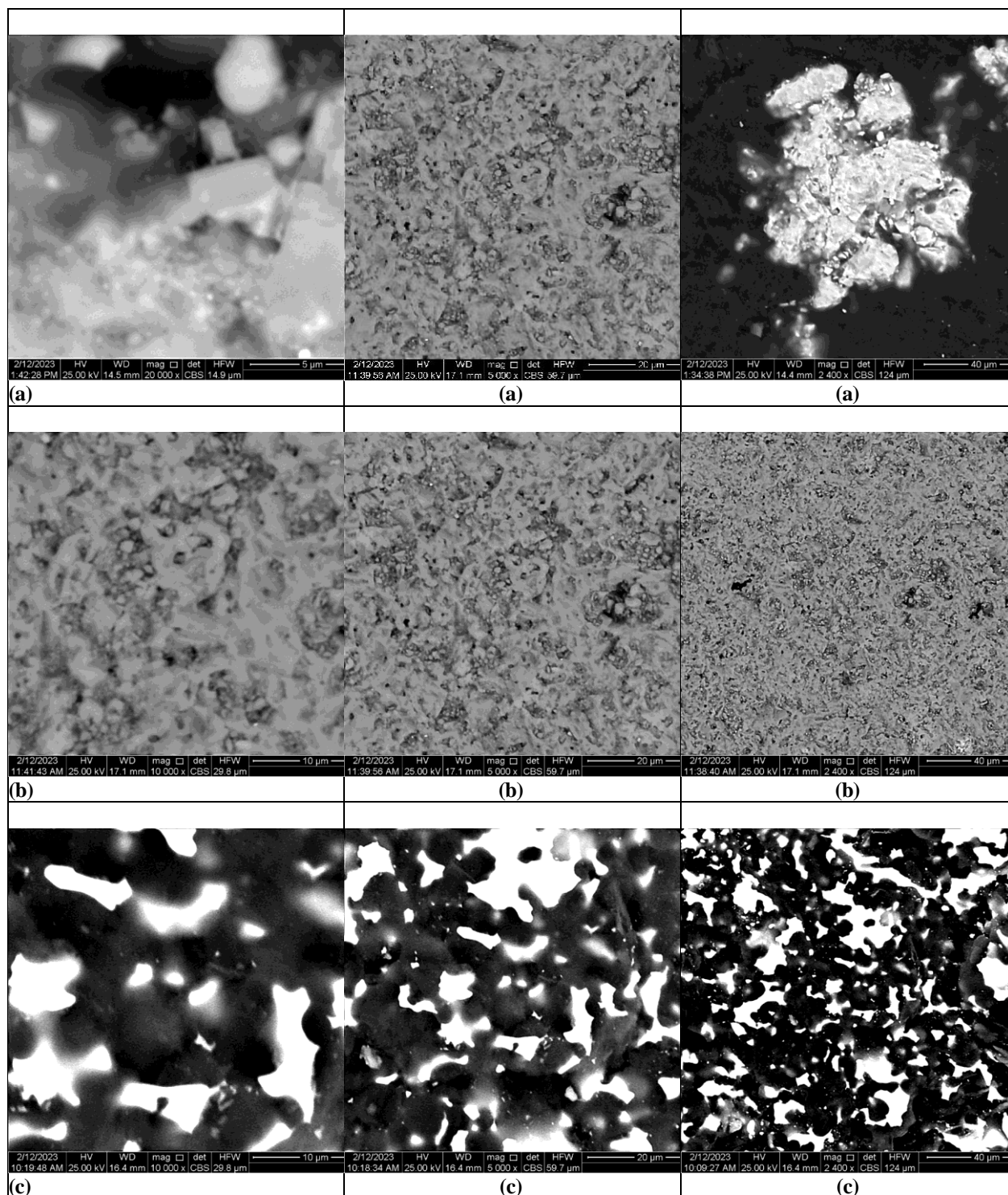


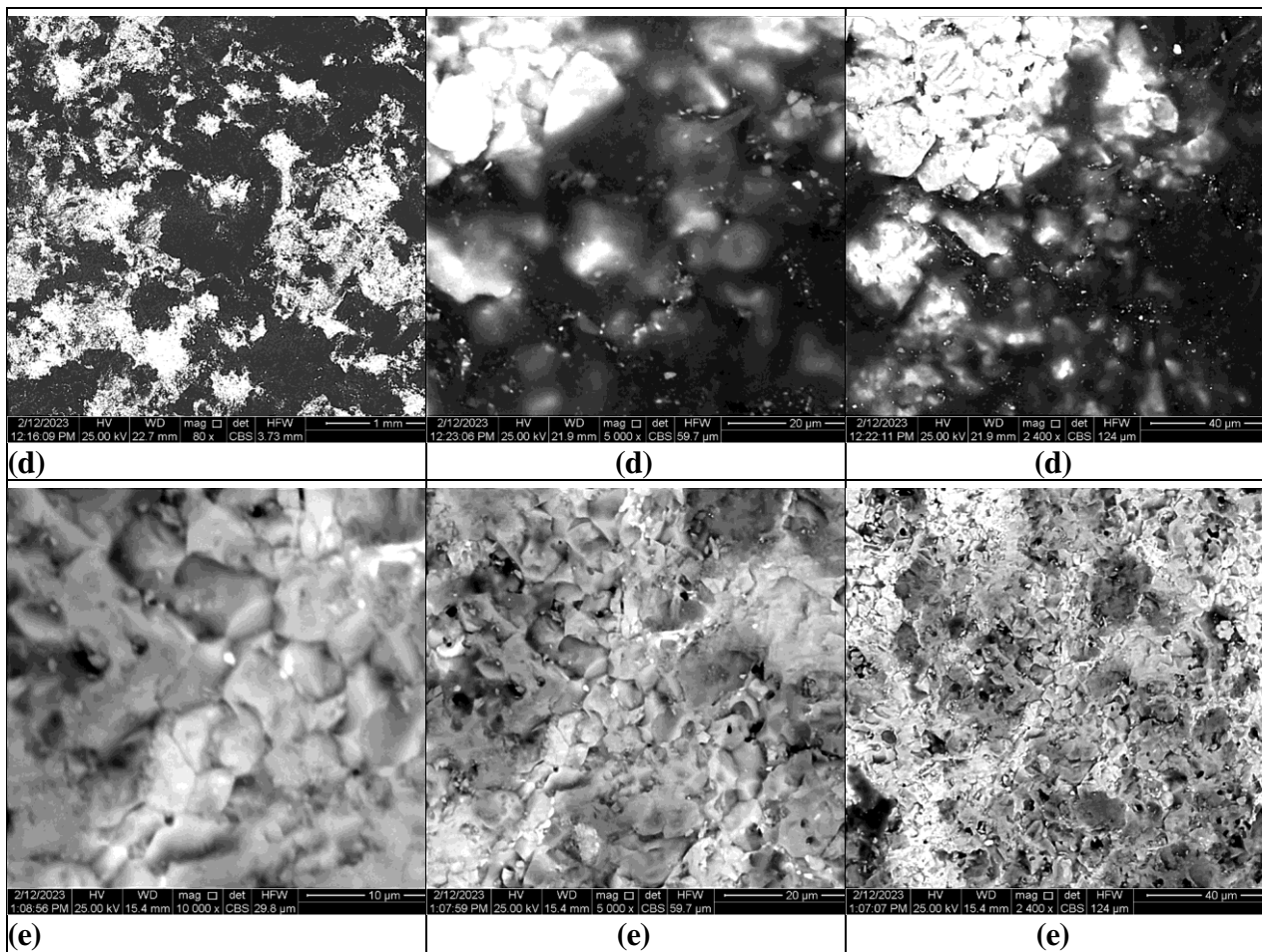
**Figure 4** Phase diagram of TiC-ZrC binary system [12–17].

**Table 3** Lattice parameters and compositions of the three phases in the 80TiC-20ZrC composite A as sintered at 1700 °C.

Parameter and Composition	As-sintered (Ti, Zr)C	TiC-rich (Ti, Zr)C	ZrC-rich (Ti, Zr)C
Lattice parameter (nm)	0.437	0.435	0.468
Composition (Vegard's law)	Ti <sub>0.91</sub> Zr <sub>0.09</sub> C	Ti <sub>0.97</sub> Zr <sub>0.03</sub> C	Zr <sub>0.94</sub> Ti <sub>0.06</sub> C
Composition estimated by the phase diagram TiC-ZrC	Ti <sub>0.9</sub> Zr <sub>0.1</sub> C	Ti <sub>0.98</sub> Zr <sub>0.02</sub> C	Zr <sub>0.89</sub> Ti <sub>0.11</sub> C

Figure 5a illustrated titanium carbide (TiC) and the Fig. 5b suggested the presence of zirconium carbide (ZrC) sintered at 1700 and 1800 °C, the relative densities reached 97.8 and 95.2 % respectively. Fig. 5c shows SEM imaging of the 80TiC–20ZrC composites A sintered at 1700 °C, there are dark and bright regions that correspond to Ti- and Zr-rich (Ti, Zr) C, respectively, at sizes of several  $\mu\text{m}$  dispersed in dark grains of Ti-rich (Ti, Zr) C with some pores. The composite had few pores, while the bright areas of Zr-rich (Ti, Zr) C is shown. These composites had relative densities of over 96%. These 80TiC–20ZrC composites A exhibited significantly high relative densities, compared to ZrC. In Fig. 5d, the SWCNTs agglomerated uniformly at the Ti and Zr-rich (Ti, Zr) C and it is with a good agreement with the work that published by Zeinedini et al., the relative densities reached 95.0–98.9% [36]. Fig. 5e a homogeneous and uniform morphology appeared of nano-tungsten carbide (NWC) of the nano-composite B, suggesting the formation of a complete solid solution of (Ti, Zr) C. The relative densities of the sintered samples were over 98%.

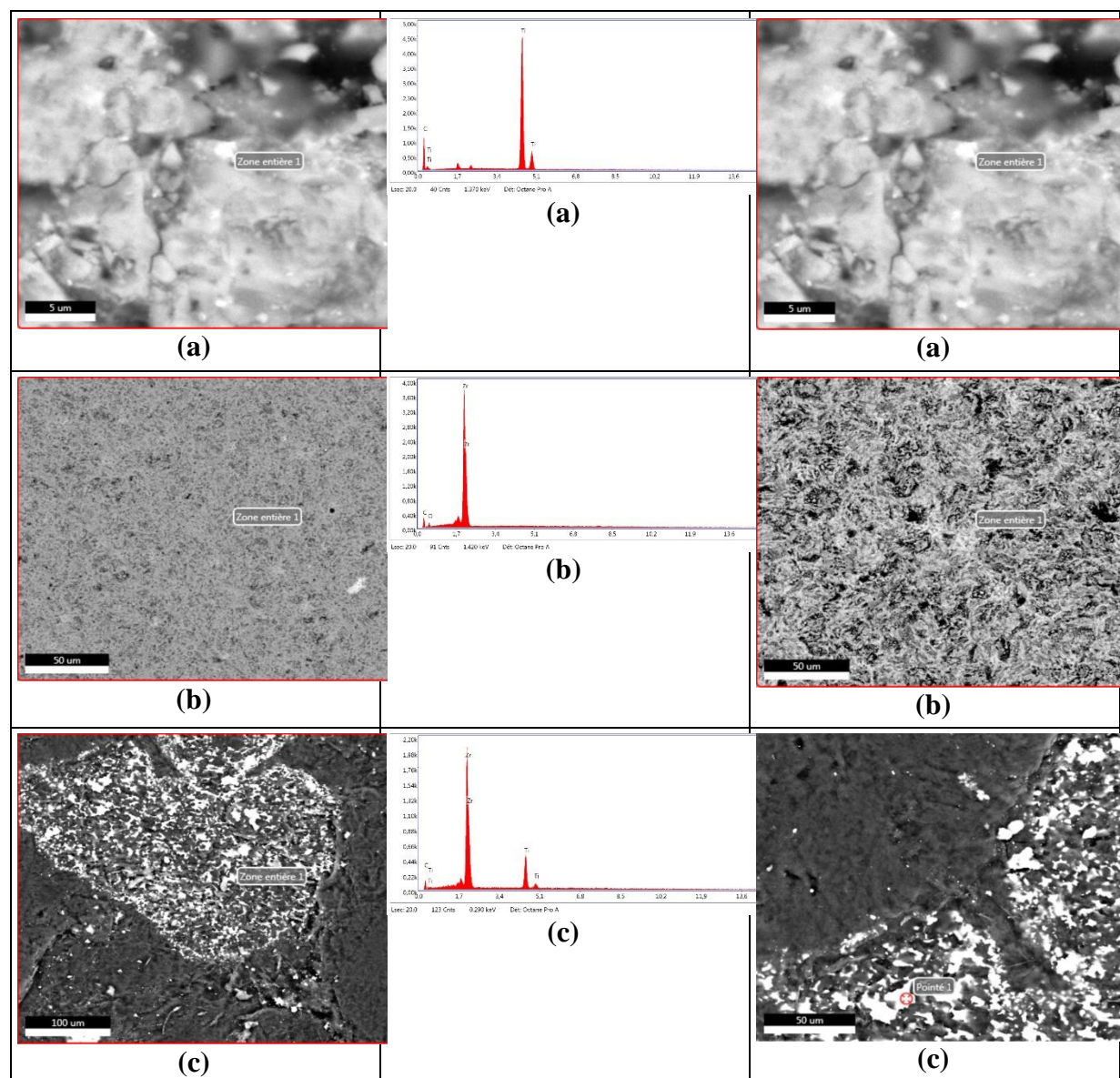




**Figure 5** High magnification microstructural representative SEM of FAST-SPS-FCT sintered samples à 1700 °C. (a)-Titanium carbide (TiC), (b)-Zirconium carbide (ZrC), (c)-Composite A, (d)-Nano-composite A, (e)- Nano-composite B.



To acquire the information on the distribution of various phases in the sintered samples, Energy-Dispersive X-ray Spectroscopy (EDS) analysis was performed on the samples. Although it is not possible to identify the phases by EDS directly, it is still very useful to detect elemental distribution of Ti, Zr, C, NWC and SWCNTs in samples. Thus, EDS analysis together with XRD results can provide more information regarding nature of FAST-SPS-FCT compacted and sintered powders. We presented in the Fig. 6 compositions in different s important regions in the composite A and nano-composite A and B. The bring idea about the structural, mechanical and ballistic performance that will be estimated by the Heisenberg model.





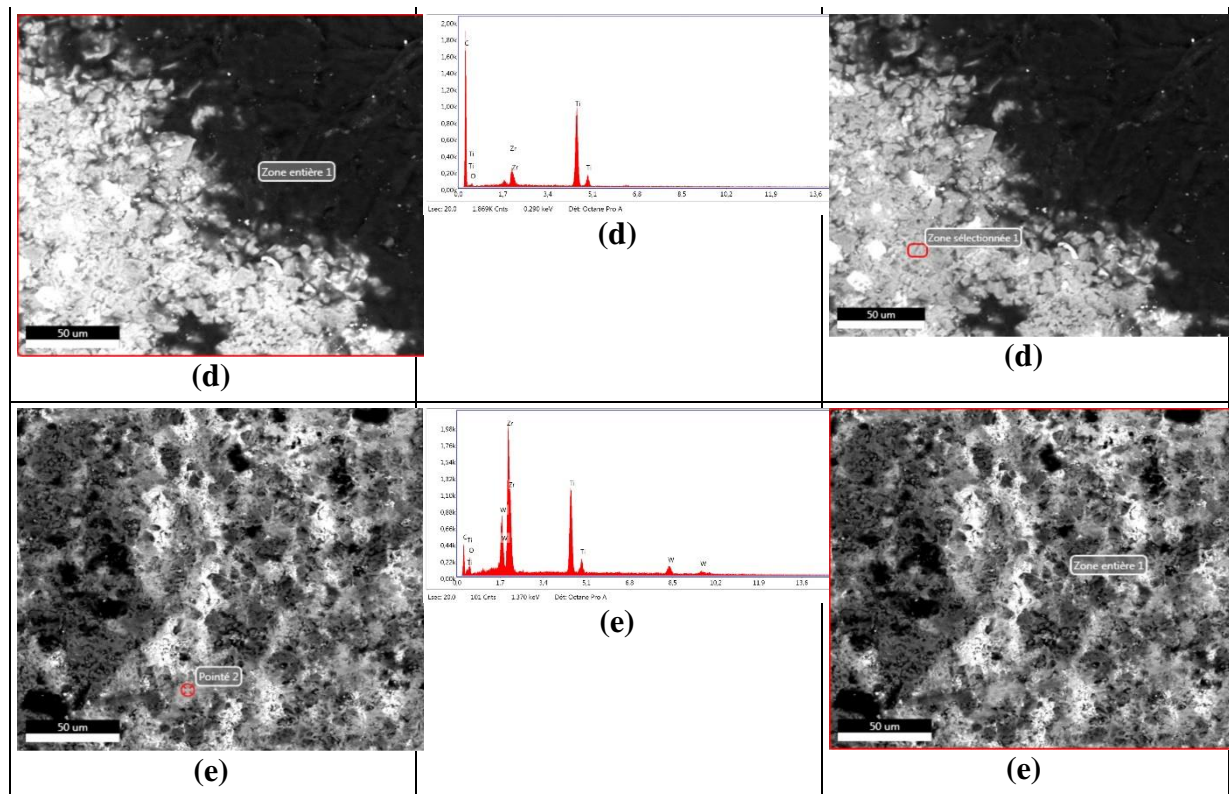


**Figure 6** High magnification micro-structural representative FESEM image their corresponding elemental distribution (Ti, Zr, C, SWCNTs and NWC) of FAST-SPS-FCT of polished and etched surface sintered at  $T=1700\text{ }^{\circ}\text{C}$ . Its higher resolution global analysis EDS pics are presented.

### 3.1.3 Mechanical and physical properties

The physical and mechanical properties were listed in the Table 4.

**Table 4** Physical parameters of the raw materials in the TiC- based nano-composites.

Parameters	TiC	ZrC	NWC	SWCNTs
E (GPa)	470	400	530–700	276
$\gamma$	0.19	0.18	270 - 950	0.2
$\alpha$ ( $\times 10^{-6} \text{K}^{-1}$ )	7.74	6.74	$6.23 \times 10^{-6} \text{C}^{-1}$	$1.0 \times 10^{-5} \text{K}^{-1}$
HV (GPa)	22.0	25.5	18.0	9.18
$K_{IC}$ ( $\text{Mpa m}^{1/2}$ )				
Theoretical density ( $\text{g/cm}^3$ )	4.94	6.73	15.8	2.25

The calculated parameters like the  $R_{st}$  parameter represents the ability of a material to resist crack propagation, further damage and loss of strength with increasing severity of thermal shock. The greater  $R_{st}$  indicates better thermal shock resistance of a material. The thermal expansion coefficient  $\alpha$  from the literature are noted in the Table 5.

**Table 5** Measured and calculated parameters of the TiC based nano-composites.

TiC based nanocomposites	E (GPa)	$\alpha$ ( $10^{-6} \text{K}^{-1}$ )	$\gamma$	$R_{st}$ ( $\mu\text{m}^{1/2} \text{ } ^\circ\text{C}$ )	Relative density (%)
Composite A	334	8.04	0.22	3194	96
NanoComposite B					95–98.9
Nano-Composite C					98
TiC	410	7.74	0.19		97.8
ZrC	400	6.74	0.18		95.2

#### 4. CONCLUSIONS

FAST-SPS-FCT technology is fast sintering process; uniform sintering; low grain growth (nano-grain materials may be prepared); compaction and sintering stages are combined in one operation; binders are not necessary; better purification and activation of the powder particles surfaces. The synthesis of composites and nanocomposites with ceramic reinforcements is easily by FAST-SPS-FCT technology. It may be produced by self-propagating high temperature synthesis (SHS) but the product present bad relative density and should be followed by FAST-SPS-FCT for better density because the kinetic of sintering is improved. The FAST-SPS-FCT technology is the way to produce composites, nanocomposite and nanostructuring of materials, also makes it possible to strengthen the material to obtain a mechanical resistance exceeding all alloys in their conventional states to protection ballistics of military vehicles. The addition of alloying elements and ceramic and the appropriate thermo-mechanical treatments are mastered and make it possible to obtain high mechanical resistance for the applications that require it. Nanostructuring and dispersion of the reinforcements will be carried out by high-energy grinding of the powder mixtures, and shaping by Spark Plasma Sintering, for the short cycles and low temperatures that the process allows. The precipitation at the origin of the structural hardening of this alloy will be the subject of particular interest. In this study it can summarize the following, according to the preliminary structural properties obtained results: 1-TiC-ZrC composites were consolidated by FAST-SPS-FCT at 1700 °C using TiC and ZrC powders. TiC-ZrC composites having TiC composition 80 vol% were densified to relative densities over 96%. The effect of SWCNTs addition on the increasing of the densities of the sintered samples in the nano-composites A, it can be explained by its uniform agglomeration. The relative densities reached 95.0–98.9%. Finally, the nano-composites B is made of TiC-ZrC-SWCNTs-NWC, also exhibited a better relative density it can estimated by the value over 98%. 2-At sintering temperatures 1700 °C, the sintered samples were mixed phases of Ti- and Zr-rich (Ti,Zr)C formed with a uniform morphology. It is no confirmed that the additions (nano-structures of SWCNTs and WC) has no effect on the lattice parameters of Ti- and Zr-rich (Ti,Zr)C because the investigations is not selected. No reaction has detected between SWCNTs (nano-composite A), nano-tungsten carbide (nano-composite B) and the composite A. The single-phase (Ti,Zr)C and the composites of Ti- and Zr-rich (Ti, Zr)C with TiC compositions of 80 vol% had relative densities greater than 97%. The theoretical and experimental ballistic performance testing of the produced nanomaterials, HV and  $K_{IC}$  measurement in addition thermo-mechanical modeling in situ FAST-SPS-FCT cycle will be performed in the near future.

#### Acknowledgments

The present work was supported by the Algerian Ministerium of Higher Education and Scientific Research (MESRS, Algiers) and the PRFU Project entitled: Synthesis, Characterization and Thermo-Mechanical Modeling of Composites, Nano-composite and Cermets for Ballistic Protection by FAST-SPS-FCT, under contract N°A11N01UN240120220005 at the University of 08 May 1945, Guelma. These supports are gratefully appreciated. I thank Pr. Djamel HAMANA and Pr. Nadhir ATTAF from the Laboratory of Phase Transition, Institute of Physics, University brother Mentouri-Constantine for the XRD investigations. I wish to thank also the Director of the School of Metallurgy and Materials Sciences, University of Badji-Mokhtar-Annaba for the SEM, EDS observations and analysis of the sintered samples. Finally, I am grateful to Pr. Frederick

Bernard and Jacques Guillome Noudem, for having made available to me the FAST-SPS-FCT Technology Sintering Apparatus-Germany and the consumable graphit dies, punches and spacer at the ENSICAEN, Caen-France and at the Laboratory ICB-Dijon-Bourgogne-France, respectively.

## References

- [1] P. J. Hazell, Advanced in ceramic armour, Military Technology - MILTECH, 2009
- [2] I. Topcu, H. O. Gulsoy, N. Kadioglu, and A. N. Gulluoglu, J. Alloys Compd 482 (2009) 516
- [3] J. R. Davis, Aluminium and aluminium alloys, ASM Handbook, ASM International, 1993
- [4] C. Suryanarayana, Prog. Mater. Sci., vol. 46 (2001) 1
- [5] E. L. Thomas, Opportunities in Protection Materials Science and Technology for Future Army Applications, John Wiley & Sons, Inc., 2012
- [6] Y. Liu, Y. Jin, H. Yu, J. Ye, Int. J. Refract. Met. Hard Mater. 29 (2011) 104
- [7] H. Zhang, J. Yi, S. Gu, Int. J. Refract. Met. Hard Mater. 29 (2011) 158
- [8] W. T. Kwon, J.S. Park, S. Kang, J. Mater. Proc. Technol. 166 (2005) 9
- [9] X. Zhang, N. Liu, C. Rong, J. Zhou, Ceram. Int. 35 (2009) 1187
- [10] L. Cheng, Z. Xie, G. Liu, W. Liu, W. Xue, J. Eur. Ceram. Soc. 32 (2012) 3399
- [11] A. Teber, F. Schoenstein, F. Tetard, M. Abdellaoui, N. Jouini, Int. J. Refract. Met. Hard Mater. 31 (2012) 132
- [12] S. Liu, W. Hu, J. Xiang, F. Wen, B. Xu, D. Yu, J. He, Y. Tian, Z. Liu, Ceram. Int. 40 (2014) 10517
- [13] S. P. Buyakova, E. S. Dedova, D. Wang, Y. A. Mirovoy, A. G. Burlachenko, A. S. Buyakov, Ceramic International 48(2022) 11747
- [14] R.G. Egres, Jr. Lee, Y. Kirkwood, J. Wagner, N. Wetzel, E. Novel flexible body armor utilizing shear thickening fluid (STF) composites. In Proceedings of the 14th International Conference on Composite Materials, San Diego, CA, USA, 2003
- [15] Y. S. Lee, N. J. Wagner, Rheo. Acta 42 (2003) 199
- [16] J. Qin, B. Guo, L. Zhang, T. Wang, G. Zhang, X. Shi, Compos. Part B 183 (2020) 107686
- [17] D. P. Kalman, R. L. Merrill, N. J. Wagner, E. D. Wetzel, ACS Appl. Mater. Interfaces 1 (2009) 2602
- [18] A. Majumdar, B.S. Butola, A. Srivastava, Mater. Des. 46 (2013) 191
- [19] S. Gorgen, M. C. Compos. Part A 94 (2017) 50
- [20] Y. Lee, E. Wetzel, N. Wagner, J. Mater. Sci. 38 (2003) 2825
- [21] M. J. Decker, C. J. Halbach, C.H. Nam, N. J. Wagner, E. D. Wetzel, Compos. Sci. Technol. 67 (2007) 565
- [22] Birringer, R.; Gleiter, H. Encyclopedia of Materials Science and Engineering; Cahn, R.W., Ed.; Pergamon Press: Oxford, UK, 1988
- [23] Gleiter, H. Nanocrystalline Materials. Prog. Mater. Sci. 33 (1989) 223
- [24] R. Dagani, Chem. Eng. News 70 (1992) 18
- [25] B. Bendjemil, E. Borowiak-Palen, A. Graff, T. Pichler, M. Knupfer, and J. Fink, Applied Physics. A78 (2004) 311
- [26] E. Borowiak-Palen, T. Pichler, G. G. Fuentes, B. Bendjemil, X. Liu, A. Graff, G. Behr, R. J. Kalenczuk, M. Knupfer, and J. Fink, Chem Commun (Camb) 1 (2003) 82
- [27] D. Selbmann, B. Bendjemil, A. Leonhardt, T. Pichler, C. Täschner, M. Ritschel, M. Knupfer, and J. Fink, Applied Physics A. 90 (2008) 637
- [28] M. Mouyane, B. Jaber, B. Bendjemil, J. Bernard, D. Houivet, J. G. Noudem, Applied ceramic Technology; 16 (2019) 1138

- [29] B. Bendjemil, J.G. Noudem, M. Mouyane, J. Bernard, Y. Guhel, and D. Houivet, *Journal of Advances in Nanotechnology*, 1 (2020) 30
- [30] B. Bendjemil, M. Mouyane, J.G. Noudem, J. Bernard, J.M. Reboul, and D. Houivet, *Journal of Advances in Nanotechnology*, 1 (2020) 14
- [31] B. Bendjemil, K. Safi, I. Kouahla, J. G. Noudem, M. Mouyane, J. Bernard, Y. Guel, and D. Houivet, *Exp. Theo. Nanotechnology* 7 (2023) 1
- [32] G. R. Anstis, P. Chantikul, B. R. Lawn, D. B. Marshall, *J. Am. Ceram. Soc.* 64 (1981) 533
- [33] X. Zhang, N. Liu, *Int. J. Refract. Met. Hard Mater.* 26 (2008) 575
- [34] V.I. Ivashchenko, P.E.A. Turchi, V.I. Shevchenko, *J. Phys.: Condens. Matter* 21 (2009) 395503
- [35] I. Borgh, P. Hedstrom, A. Blomqvist, J. Agren, J. Odqvist, *Acta Mater.* 66 (2014) 209
- [36] A. Zeinedini, M. M. Shokrieh, A. Ebrahimi, *Theoretical and applied Fracture Mechanics*, 94 (2018) 84
- [37] M. J. Bronikowski, P. A. Willis, D. T. Colbert, R. E. Smalley, *Journal of Vacuum sciences and technology A*, 19 (2001) 564
- [38] M. Moser, S. Dine, D. Vrel, L. Perrière, R. Pirès-Brazuna, *Materials*, 15 (2022) 5416